Front. Phys., 2014, 9(2): 137–152
DOI 10.1007/s11467-013-0359-z

REVIEW ARTICLE

Quantum tunneling of ultracold atoms in optical traps

Jian-Hua Wu, Ran Qi, An-Chun Ji, Wu-Ming Liu†

Beijing National Laboratory for Condensed Matter Physics, Institute of Physics, Chinese Academy of Sciences, Beijing 100190, China

E-mail: †*wmliu@aphy.iphy.ac.cn*

Received April 18, 2013; accepted May 26, 2013

We review our theoretical advances in quantum tunneling of Bose–Einstein condensates in optical traps and in microcavities. By employing a real physical system, the frequencies of the pseudo Goldstone modes in different phases between two optical traps are studied respectively, which are the crucial feature of the non-Abelian Josephson effect. When the optical lattices are under gravity, we investigate the quantum tunneling in the "Wannier–Stark localization" regime and "Landau–Zener tunneling" regime. We finally get the total decay rate and the rate is valid over the entire range of temperatures. At high temperatures, we show how the decay rate reduces to the appropriate results for the classical thermal activation. At intermediate temperatures, the results of the total decay rate are consistent with the thermally assisted tunneling. At low temperatures, we obtain the pure quantum tunneling ultimately. And we study the alternating-current and direct-current (ac and dc) photonic Josephson effects in two weakly linked microcavities containing ultracold two-level atoms, which allows for direct observation of the effects. This enables new investigations of the effect of many-body physics in strongly coupled atom-cavity systems and provides a strategy for constructing novel interference devices of coherent photons. In addition, we propose the experimental protocols to observe these quantum tunneling of Bose–Einstein condensates.

Keywords quantum tunneling, Josephson effect, Landau–Zener tunneling, atom-cavity

PACS numbers 03.75.Lm, 05.30.Jp, 42.50.Pq, 67.85.De

Contents

1 Introduction

Quantum tunneling refers to the quantum mechanical phenomenon where a particle tunnels through a barrier that it classically could not overcome. This plays a primary role in several physical phenomena, such as the nuclear fusion that occurs in main sequence stars [1], radioactive decay, and has important applications to modern devices such as the tunnel diode [2], cold emission and STM. Quantum tunneling was developed from the research of radioactivity [3], which was discovered by Henri Becquerel [4] in 1896. Marie and Pierre Curie earned the Nobel Prize in Physics in 1903 for further study of Radioactivity [4].

Hund was the first to take careful notice of tunneling in 1927 when he was calculating the ground state of the double-well potential [4] which is a very important model to study quantum tunneling. In 1995 the realization of Bose–Einstein condensates (BECs) brings an ideal tool to study this ancient problem. The tunneling of BECs differs in two aspects from the traditional quantum tunneling, one is the macroscopic dimensions of the BECs, and the other is that the atom–atom interactions plays an important role in this quantum many-body system. In the last few years, the tunneling between trapped Bose–

Einstein condensates has attracted the huge attention of many theorists and significant research effort has been devoted to it [5–27].

The Josephson effect is a quantum tunneling phenomenon of supercurrent first discovered in superconducting Josephson junction, the junction consists of two superconductors coupled by a weak link which is weak enough only allow a slight overlap of the electron pair wave functions of the two superconductors. The weak link can consist of a thin insulating barrier (S-I-S), a short section of non-superconducting metal (S-N-S), or a physical constriction that weakens the superconductivity at the point of contact (S-s-S).

The Josephson effect was named after Brian David Josephson, who predicted the electron can cross insulation without voltage at the both ends of the tunnel junction and forming current when the thickness of the insulating layer is only a few dozen Å in 1962 when he was still a graduate student, it seems that the insulating layer also become superconductors. Beginning with Josephson's original paper [28], the Josephson effect has become a exemplification of the phase coherence representation in a macroscopic quantum system. Thanks to the rapid experimental development in cold atom physics, the Josephson junction has been came ture for the trapped Bose–Einstein condensates (BEC) of ^{87}Rb [29] and ^{23}Na [30]. The Josephson effect has many applications, superconducting quantum interference device (SQUID)Is one of them, which is the instrument to accurately measure the magnetic field. The contribution of Josephson Effect made the superconducting applications valuable, at the same time it led to a series of interesting physical problems.

In this article, we review our theoretical advances in quantum tunneling of Bose–Einstein condensates in optical traps. We give an detailed introduction of the quantum tunneling between $F = 2$ spinor Bose–Einstein condensates in double optical traps which called non-Abelian Josephson Effect in Section 2. Section 3 is devoted to investigate the quantum tunneling of Bose–Einstein condensates in optical lattices under gravity. and in Section 4, we discuss the Josephson Effect for photons of Bose–Einstein condensates in two weakly linked microcavities. Finally, we summarize our results.

2 Quantum tunneling in double optical traps

The Josephson effect can be successfully explained by using the principle of quantum mechanical tunneling. First of all, we taken the two superconductors as two potential wells, and then the insulating layer between the two wells correspond to construct a barrier. When the layer is thick enough, the electron pair in the two conductors are independent. With the thinning of the insulating layer, the two wave functions of the conductors begin to overlap which provides quantum correlations on different conductors and makes the electron pairs passed through the insulating layer to reach another conductor smoothly, thereby forming supercurrent. If both ends of the superconductor coupled with DC voltage, electrons are able to shuttle back and forth in the insulating layer and formed AC current. These predictions were soon confirmed by the experimental observation of Anderson.

However, most of the studies about the Josephson effect focus on the Abelian case. The Abelian Josephson effect giving rise to a weak interaction between the macroscopic states of each superconductor which separated by a thin layer of normal material. The interaction mentioned above allows a tunneling-mediated current flow across the thin layer. The Abelian Josephson effect in terms of a junction of two systems with spontaneously broken Abelian symmetry [31, 32]. The non-Abelian Josephson effect, theoretically speaking, is universal in nature and covering many topics from particle physics to condensed matter physics. Esposito *et al.* who extended the Abelian case to the non-Abelian case in field theoretic language recently [33]. The non-Abelian Josephson effect come out in a junction with non-Abelian symmetries broken spontaneously which usually contains multicomponent order parameters. The symmetry in non-Abelian case will give rise to more than one kind of tunneling modes [34]. These tunneling modes can be distinguished by the excitation of pseudo Goldstone bosons which have small but finite masses [33].

2.1 Ground state

As shown in Fig. 1, we consider a homogenous spin-2 Bose gas system with s-wave interaction. We describe this system by the following mean field free energy:

$$F(\psi) = \frac{1}{2}[j_0(\psi^\dagger\psi)^2 + j_1\langle \boldsymbol{f}\rangle^2 + \frac{j_2}{5}|\Theta|^2] - \mu\psi^\dagger\psi \qquad (1)$$

where j_0, j_1 and j_2 are interaction strengths of different spin channels related to the scattering length, $\psi = (\psi_2, \psi_1, \psi_0, \psi_{-1}, \psi_{-2})^{\mathrm{T}}$ is the order parameter of the system, $\langle \boldsymbol{f}\rangle = \psi^\dagger \boldsymbol{f}\psi$ is the mean value of the spin operator and

$$\Theta = \sum_{a=-2}^{2}(-1)^a\psi_a\psi_{-a} \qquad (2)$$

is the expression of a single pair of identical spin-2 particles. By minimizing this free energy we can get the

ground state configuration. There are couple of distinct phases in this system [36, 35]. The low-lying excitation spectrum and the symmetry of each phase will be analyzed under zero magnetic field.

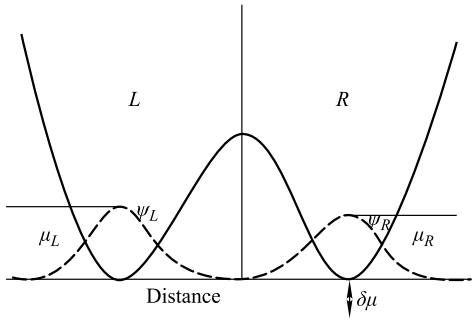

Fig. 1 The experimental schematic of a spin-2 Bose gas trapped in a double well with chemical potentials μ_L of left and μ_R of right trap, which initially satisfy $\mu_L = \mu_R$. To drive Josephson effect, we add a small distortion $\delta\mu$ to μ_R.

Antiferromagnetic phase: When the magnetic field is inexistence, there is only one kind of antiferromagnetic phase are satisfied when $j_2 < 0$ and $j_1 - j_2/20 > 0$. The corresponding ground state configuration is degenerate with reference to five continuous variables, and this will lead to five masses Goldstone modes [36]. Four of these modes of the free energy correspond to the $U(1) \times SO(3)$ symmetry. The extra degeneracy besides the symmetry will be removed when the quantum fluctuation is considered which is correct only on the mean field level.

Ferromagnetic phases: When $j_1 < 0$ and $j_1 - j_2/20 < 0$, there are two kinds of ferromagnetic phases are actively favored. The configurations of the corresponding ground state are given by

$$\begin{aligned}\psi &= \sqrt{n}\mathrm{e}^{\mathrm{i}\theta}(0,1,0,0,0)\\ \psi &= \sqrt{n}\mathrm{e}^{\mathrm{i}\theta}(1,0,0,0,0)\end{aligned} \tag{3}$$

where θ is an arbitrary global phase and $n = \mu/(j_0+4j_1)$ is the particle density. It is clearly that these ground states have a $U(1)$ symmetry and will leads to only one massless Goldstone mode. Accordingly, two uncoupled systems have a $U(1)\bigotimes U(1)$ symmetry. When a weak coupling is applied, this symmetry will softly break into a $U(1)$ diagonal symmetry. This type of symmetry breaking corresponds to an Abelian Josephson effect, and the low-lying excitation spectrum corresponding to this state has been derived as $\omega_k = \sqrt{\epsilon_k(\epsilon_k + 2g_4 n)}$ [35], where $g_4 = j_0 + 4j_1$ and $\epsilon_k = k^2$. We should notice that when coupling is applied, this Goldstone mode will break into two modes: one pseudo Goldstone mode and one zero energy mode. This pseudo Goldstone mode has a small but finite gap and leads to a density mode fluctuation in d.c. Josephson current.

Cyclic phase: When $j_1 > 0$ and $j_2 > 0$, the ground state configuration is given by

$$\psi = \sqrt{\frac{n}{2}}\left(\frac{\mathrm{e}^{\mathrm{i}\theta_2}}{\sqrt{2}}, 0, \mathrm{e}^{\mathrm{i}\theta_0}, 0, \frac{\mathrm{e}^{\mathrm{i}\theta_{-2}}}{\sqrt{2}}\right) \tag{4}$$

where $n = \mu/j_0$ is the particle density in each well and the global phase of the ground state satisfy $\theta_2 + \theta_{-2} - 2\theta_0 = \pi$ [36, 37]. One can see that the ground state of cyclic phase is mapped to a tetrahedron on the unit sphere by using the Schwinger boson representation [38]. The ground state of cyclic phase leads to four Goldstone modes on account of a full $U(1) \times SO(3)$ degeneracy. We will reveal that these modes will also lead to non-Abelian Josephson effect [34].

2.2 Non-Abelian Josephson effect

As shown in Fig. 1, we will analyze the non-Abelian Josephson effect of a spin-2 Bose–Einstein condensate system in a double-well optical trap. We suppose that the coupling between the Bose gas in each well is very weak for the energy barrier between the two wells is strong enough and the overlap of the ground state wave functions (which we denote as $\varphi_L(\boldsymbol{x})$ and $\varphi_R(\boldsymbol{x})$ in left and right well) can be safely neglected. We take the same mode function for all five spin components, this approximation called the single mode approximation which is a widely used approximation and it is valid when the spin interaction is symmetric. The system can be described by the following coupled potential V_c under these assumptions

$$V_c = F(\psi_L) + F(\psi_R) - J(\psi_L^\dagger\psi_R + \psi_R^\dagger\psi_L) \tag{5}$$

where J is the coupling parameter and ψ_L and ψ_R are the order parameter of the system in left and right well respectively. Because we will only be interested in the d.c. Josephson effect which captures the essence of the non-Abelian symmetry breaking as simple as possible, we take the same chemical potential for the Bose gas in each well. The dynamic equations of the condensate is

$$\begin{aligned}\mathrm{i}\frac{\mathrm{d}}{\mathrm{d}t}\psi_{aL} &= \frac{\delta V_c}{\delta\psi_{aL}^*}\\ \mathrm{i}\frac{\mathrm{d}}{\mathrm{d}t}\psi_{aR} &= \frac{\delta V_c}{\delta\psi_{aR}^*}\end{aligned} \tag{6}$$

by using it we can get the equation of motion of the Josephson current and analyze the pseudo goldstone modes in each phase. However, the symmetry of the ground state in ferromagnetic phase only leads to an Abelian Josephson effect as we have mentioned above, which is not discussed in our paper. We just analyze the antiferromagnetic phase and cyclic phase which are

important realizations of non-Abelian Josephson effect consequently.

Antiferromagnetic phase: The ground state of antiferromagnetic phase is

$$\psi_L = \psi_R = \sqrt{\frac{n}{2}}(1,0,0,0,1) \tag{7}$$

we linearized the equation of motion around the ground state Eq. (7) to obtain the pseudo goldstone modes, and then we get $n = (\mu + J)/(c_0 + c_2/5)$ by minimizing the potential V_c under the above ground state. We obtain the linearized equations of the fluctuations in this phase and analyze the excitation spectrum with this ground state configuration.

(i) The $m = 0$ mode. We can obtain the equation of motion of $m = 0$ mode as

$$\mathrm{i}\frac{\mathrm{d}}{\mathrm{d}t}\phi_{0L} = (-\frac{j_2}{5}n + J)\phi_{0L} + \frac{j_2}{5}n\phi_{0L}^* - J\phi_{0R} \tag{8}$$

and the equation of ϕ_{0R} is similarly. It corresponds to an Abelian Josephson current for this mode is decoupled from others. We obtain the eigenenergies of this mode by solving Eq. (8), one is $\omega_0 = 2\sqrt{J(J + \frac{2|j_2|n}{5})}$ corresponding to a pseudo Goldstone mode and the other is zero corresponding to a massless Goldstone mode.

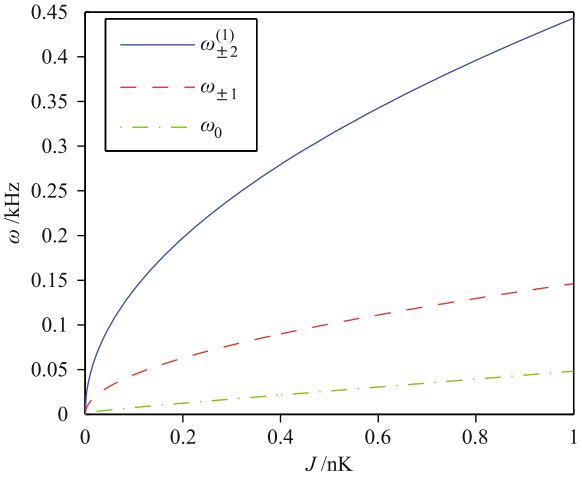

Fig. 2 The frequencies of the pseudo Goldstone modes as a function of coupling parameter J in the case of antiferromegnetic phase. All the frequencies is proportional to $\sqrt{J}$ when J approaches zero and the dependence on J becomes linearizing when J is large compared to the interaction energy. Reproduced from Ref. [34], Copyright © 2009 American Physical Society.

(ii) The $m = \pm 1$ coupled modes. The coupled equations of $m = \pm 1$ modes are shown in the following

$$\mathrm{i}\frac{\mathrm{d}}{\mathrm{d}t}\phi_{1L} = [n(j_1 - \frac{j_2}{5}) + J]\phi_{1L} + n(j_1 - \frac{j_2}{5})\phi_{-1L}^* - J\phi_{1R}$$
$$\mathrm{i}\frac{\mathrm{d}}{\mathrm{d}t}\phi_{-1L} = [n(j_1 - \frac{j_2}{5}) + J]\phi_{-1L}$$
$$+n(j_1 - \frac{j_2}{5})\phi_{1L}^* - J\phi_{-1R} \tag{9}$$

and a similar suit of equations of $\phi_{\pm 1R}$. The solution of these equations involves two pseudo Goldstone modes with the same gap of

$$\omega_{\pm 1} = 2\sqrt{n(j_1 - j_2/5)J + J^2} \tag{10}$$

(iii) The $m = \pm 2$ coupled modes. The coupled equations of $m = \pm 2$ modes are similar to the ones of $m = \pm 1$ case. Here and after, we will not list the detailed coupled equations of motion but just give the result. The solution of $m = \pm 2$ equations give two pseudo Goldstone modes with energy gap

$$\omega_{\pm 2}^{(1)} = 2\sqrt{n(j_0 + \frac{j_2}{5})J + J^2}$$
$$\omega_{\pm 2}^{(2)} = 2\sqrt{n(j_1 - \frac{j_2}{20})J + J^2} \tag{11}$$

As we all can see that there are totally five pseudo Goldstone modes with four different gaps in this phase which accord with our analysis of the ground state degeneracy. The dependence of the above frequencies on coupling parameter J are shown in Fig. 2. We expect that in future experiments the above modes of fluctuations can be observed in this system. With reference to ^{87}Rb system, under typical experimental condition, the value of interacting strengths are given as [39]: $j_1 n$: 0–10 nK, $j_2 n$: 0–0.2 nK and $j_0 n$ about 150 nK. We assume that the coupling parameter J is much smaller than the interaction energy of the condensate given as about 0.1 nK according to the weak coupling limit. With this understanding, we can obtain the frequencies of the fluctuation related to the antiferromagnetic phase, which is of order 100 Hz. In current experiments, the measurement of fluctuations on this characteristic time scale (about 10 ms) is accessible.

Cyclic phase: We can obtain the pseudo Goldstone modes for the cyclic phase by following the same procedure in the antiferromagnetic phase.

(i) The $m = \pm 1$ coupled modes. As is known to all, there are two massless Goldstone modes with the same energy [35]. We find that by solving the equation of motions each of them leads to a pseudo Goldstone mode with a gap:

$$\omega_{\pm 1} = 2\sqrt{J^2 + 2j_1 nJ} \tag{12}$$

The four pseudo Goldstone modes in this phase is consistent with our previous analysis on the symmetry. In a condensate of ^{85}Rb atoms, these kinds of fluctuations are expected to be realized [36]. Under typical experimental condition, the value of interacting strengths based on the

current estimates of scattering lengths are given as: $j_1 n$: 0–20 nK, $j_2 n$: 0–0.6 nK and $j_0 n$ about 600 nK. In the mentioned cases, we can also estimate the d.c. Josephson frequencies in cyclic phase, the frequencies is about 100–300 Hz. In Fig. 3, the dependence of the above frequencies on coupling parameter J is shown.

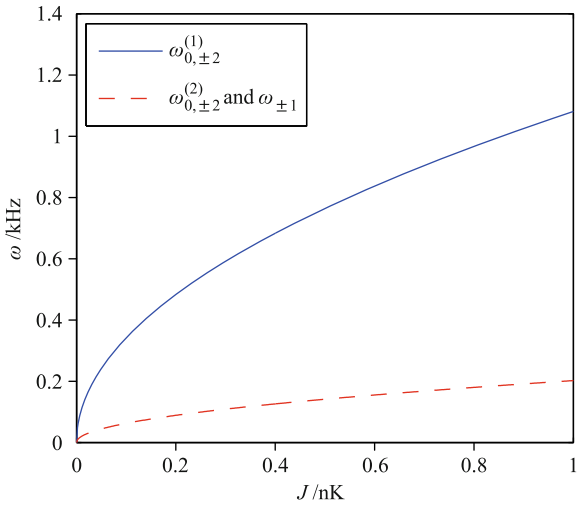

Fig. 3 The frequencies of pseudo Goldstone modes as a function of coupling parameter J in the case of cyclic phase. The dependence on J is similar to the case in antiferromegnetic phase. However, there are two degenerate modes $\omega^{(2)}_{0,\pm 2}$ and $\omega_{\pm 1}$ in this case, which are originated from the two degenerate Bogoliubov modes in the uncoupled system. Reproduced from Ref. [34], Copyright © 2009 American Physical Society.

(ii) The $m = \pm 2, 0$ coupled modes. We have found that in the corresponding uncoupled system [35] each Goldstone mode breaks into one massless mode and one pseudo Goldstone mode. Since there are two Goldstone modes, we find two pseudo Goldstone modes in the uncoupled system which energy given by

$$\omega^{(1)}_{0,\pm 2} = 2\sqrt{J^2 + j_0 n J}$$
$$\omega^{(2)}_{0,\pm 2} = 2\sqrt{J^2 + 2 j_1 n J} \qquad (13)$$

2.3 Experimental protocol and signatures

How to design an experimental protocol to observe this novel non-Abelian effect in experiments? To our knowledge, in any real physical system, this effect has not been explicitly spelled out, which is what we attempt to do here. First of all, we need a system of multi-component order parameter which has a non-Abelian symmetry in the ground state to generalize to the non-Abelian junction in experiments. In sharp contrast with magnetic trap, the spin of the alkali atoms is essentially free in an optical trap [40–42]. The scenario of our non-Abelian construction would properly provided by this spinor nature. We now introduce the system which contain a spinor atomic BEC in a double-well optical traps briefly. The essence of the non-Abelian effect has not been captured though the dynamical tunneling properties of spin-1 and "pseudo spin-1/2" bonsonic systems have been calculated [43–47]. Due to the non-Abelian symmetry breaking we focus on the pseudo Goldstone modes, which is at the heart of Josephson effect. Compared with the spin-1 system, the spin-2 system has possible advantages in the sense that the symmetry properties are much richer to explore the non-Abelian effect. We should note that some elements of the symmetry group are hidden in the ground state in spin-1 system. For example, the symmetry group of ground state is $U(1)\times S(2)$ in the polar state of spin-1 system, which is a subgroup of the symmetry group of the Hamiltonian $U(1)\times SO(3)$ [42]. In low spin system, some rotation in the symmetry group of the Hamiltonian will leave the ground state unchanged and do not contribute to Goldstone modes, that is the reason why this happens. In contrast with the low spin system, in the antiferromagnetic and cyclic phase of spin-2 condensate, the full $U(1) \times SO(3)$ symmetry is preserved in the ground state configuration, which except for some specific values of the parameter [38].

In Fig. 1, the simple experimental set up of a spin-2 Bose gas trapped in a double well potential is illustrated. With the following steps we can detect the d.c. non-Abelian Josephson current. To initiate a density oscillation in the system is the first step. This can be realized by slightly changing the depth of one well and then tuning it back, which will cause a small imbalance in chemical potential ($\mu_R \to \mu_R + \delta\mu$) between the two wells. The second step is to detect the time dependence in different spin component of the particle numbers. Such kind of detection can be realized by two steps, the first steps is spatially separating different spin component with a Stern–Gerlach method during time of flight after switching off the trapping potential. Then, by the absorption imaging method, the number of atoms in each spin component which related to the respective spatial density distributions can be evaluated. By following these steps, we can measure the density oscillation of each spin component which are coupled together as a result of the non-Abelian symmetry of the system. The dependence of the oscillation frequencies on J can be realized by varying the barrier between the two wells and repeating the above measurement.

The condensates of ^{87}Rb atom in $F = 2$ state, in mean field theory, are predicted to be polar ($j_2 < 0$ and $j_1 - j_2/20 > 0$), but close to the border to cyclic phase ($j_1 > 0$ and $j_2 > 0$) [36]. In recent experiment, polar behavior in the $F = 2$ ground state of ^{87}Rb condensate has been observed [39]. As a result, we look forward to the

pseudo Goldstone modes of the antiferromegnetic phase could be observed in experiments. We have mentioned above that the value of interacting strengths under typical experimental condition are given as [39]: $j_0 n$ about 150 nK, $j_1 n$: 0–10 nK and $j_2 n$: 0–0.2 nK, which leads to the fluctuation time scale of about 10ms. The measurement, on this time scale, is completely accessible in $F = 2$ spinor Bose–Einstein condensates of ^{87}Rb system within recent experimental technique [39, 48]. For purpose of observing this dynamical oscillation in experiment clearly, the temperature of the system should be lower than the gap of the pseudo Goldstone modes, which is about 1–10 nK. We expect that such kind of measurement performed in a system of the cyclic phase will be realized in a condensate of ^{85}Rb atoms in the near future [36].

3 Quantum tunneling in optical lattices

In this part, we investigate another type of quantum tunneling by considering two different Bose–Einstein condensates: one is in optical lattices under gravity in the regime of "Wannier–Stark localization", metastable states can exhibit interesting decay behavior in this regime; the other is in the Landau–Zener regime. Landau–Zener tunneling is a very basic quantum phenomena, It describes the quantum tunneling between adjacent energy levels of a system which under linear drive. This phenomenon was found by Landau, Zener and Stueckelberg in 1932 independently, and also known as the Landau–Zener–Stueckelberg tunneling. This tunneling generally exist in many systems, and has a wide range of applications, such as chemical reaction systems, nuclear physics, and spin system. Although this phenomenon was found over seventy years, but the passion for it has not reduced. This phenomenon continues to have been observed in some physical systems recently, such as cold-atom systems, superlattices and superconducting devices. We calculate the total decay rate in the Wannier–Stark regime for all temperatures [49] by using the periodic instanton method [50].

We will differentiate two tunneling regimes of BEC in optical lattices under gravity: (i) tunneling between spatially localized states in each individual wells, which corresponding to tunneling between Wannier–Stark localized states; and (ii) tunneling between spatially delocalized states in different Bloch bands, which usually called Landau–Zener tunneling is only the adiabatic approximation to the regime [51, 52]. When any external force is absent, the tunneling between the localized states is what creates the Bloch bands, which only survive for weak external forces. Thus the system is in the Landau–Zener tunneling regime for a small force, whereas the system shifts to the Wannier–Stark regime for a large force. The tunneling which related Landau–Zener tunneling has been measured Experimentally [55]. Here we will investigate the tunneling in Wannier–Stark regime theoretically.

3.1 Wannier–Stark tunneling

Weakly Bose–Einstein condensates were trapped in 30 wells [51] or 200 wells [52] under gravity in experiments. Approximately 10^3 atoms were contained in each well with the peak densities matching the Gaussian profile. The wells are oriented vertically, so the interwell gravitational potential drive the atoms undergo coherent motion. The gravitational potential mgz also determines the chemical potential difference between adjacent wells. Figure 4 describes the optical potential combined with the gravitational trapping potential. The corresponding Hamiltonian of this system is

$$H = \frac{P^2}{2m} + U_d(x,y)\sin^2(\frac{2\pi}{\lambda}z) + mgz \tag{14}$$

where m is the atomic mass, P is the momentum operator, λ is the wavelength of light of the optical potential, $U_d(x,y)$ is the depth of each well, and mgz is the gravity potential.

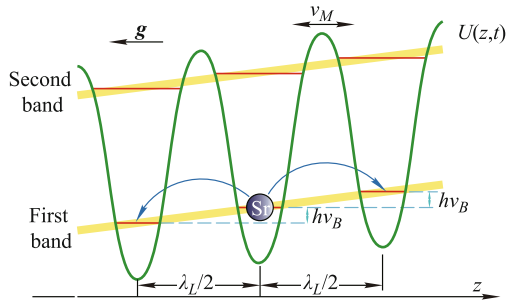

Fig. 4 Intraband site-to-site tunneling resonantly sets in when the temporal modulation frequency ν_m of the lattice phase is an integer multiple of the Bloch frequency ν_B, which corresponds to the potential energy between adjacent sites due to the gravity acceleration g. Reproduced from Ref. [54], Copyright © 2008 American Physical Society.

For definiteness and to simplify the analysis, we focus on the parameter region (defined quantitatively below) in which atoms decay from a localized state (ground or excited) in one well to the continuum and consider tunneling of atoms from a metastable state with finite energy E through a potential barrier $U(z)$. We require $mg < \frac{4\pi}{\lambda}U_d(x,y)$ to guarantee the existence of the well. We use the same definition of Δ as in Fig. 1 of Ref.

[51], $\Delta > 0$ means that the atoms can decay to infinity via a single tunneling. In this case, we can approximate a single well of the lattices by a cubic potential, where $\Delta = \Delta_{top} - [U_d(x,y) - E]$, E is the energy of any metastable state and $\Delta_{top} = mg\lambda/2$ is the difference between tops of two nearby maxima of the optical lattices under gravity. When $E = E_0$, the excited metastable state will reduce to a metastable ground state, where E_0 is the lowest metastable state. Under the circumstances, we can use an effective potential $U(z)$ to approximate the optical lattices under gravity.

The periodic instanton method is an efficient tool to study quantum tunneling of metastable states in quantum field theories. The periodic instanton represents the pseudo-atom configuration responsible for tunneling under the energy E barrier. A metastable state tunneling out from a potential $U(z)$ can be treated as motion in the corresponding inverted potential with imaginary time $\tau = \mathrm{i}t$, where

$$\begin{aligned} U(z) &= U_0 + \frac{U_d(x,y)\cos\theta_0}{2}(\frac{4\pi}{\lambda}z + \theta_0)^2 \\ &\quad + \frac{U_d(x,y)\sin\theta_0}{3}(\frac{4\pi}{\lambda}z - \pi + \theta_0)^3 \\ U_0 &= -U_d(x,y)\cos\theta_0 + U_d(x,y)(\pi - \theta_0)\sin\theta_0 \\ \theta_0 &= \arcsin\frac{mg\lambda}{4\pi U_d(x,y)} \end{aligned} \tag{15}$$

In Euclidean space-time, The Euler–Lagrange equations lead to

$$\frac{1}{2}m(\frac{\mathrm{d}z}{\mathrm{d}\tau})^2 - U(z(\tau)) = -E \tag{16}$$

where $z_p(\tau) = z_3 + (z_2 - z_3)\mathrm{sn}^2(u|k)$ is the corresponding "periodic instanton" solution with period $\mathcal{T}$, and $z_p(\tau + \mathcal{T}) = z_p(\tau)$, where $z_1(E) > z_2(E) > z_3(E)$ denote three roots of the equation $V(z) = E$. This case is equal to a special coordinate with periodic boundary conditions [50]; $\mathrm{sn}(u|k)$ denotes a Jacobian elliptic function with the modulus $k = \sqrt{\frac{z_2 - z_3}{z_1 - z_3}}$, where

$$\begin{aligned} u &= \gamma(k')\tau, \quad k' = \sqrt{1 - k^2} \\ \gamma(k') &= \sqrt{\frac{32\pi^3 U_d(x,y)\cos\theta_0(z_1 - z_3)}{3m\lambda^3(\pi - 2\theta_0)}} \end{aligned}$$

is complementary modulus of k [49].

Because the velocity of instanton vanishes at the turning points z_2 and z_3, the Feynman propagator of path integral is divergent for previous periodic instanton solution. We can smoothe this singularity out by turning point integrations of $\mathrm{d}z_2$ and $\mathrm{d}z_3$ with $\tau_2 - \tau_3 = 2\beta$. Further, we use their leading WKB approximations to replace the wave functions $\psi_E(z_2)$ and $\psi_E(z_3)$, then expand the action in powers of $z_2 - z_p(\beta)$ up to the second order, which corresponds to the one loop approximation. One instanton contribution to the transition amplitude A_1 can be obtained by using the one loop expansion of the action and completing the turning point integration. Similarly, jth instanton contribution A_j can be obtained, etc.

We can use the imaginary part of the complex energy E to define the decay rate Γ of the quantum metastable states, $\Gamma = \frac{2}{\hbar}ImE$. Let us denotes an eigenstate of the Hamiltonian H with energy E by $|\Psi\rangle$. Consider the transition amplitude A_t from $|\Psi\rangle$ to $|\Psi\rangle$, which means the "survival probability" of $|\Psi\rangle$, over Euclidean time 2β in the present of quantum tunneling,

$$A_t = \langle\Psi|\mathrm{e}^{-2H\beta}|\Psi\rangle = \mathrm{e}^{-2E\beta} \tag{17}$$

where $\beta = \mathrm{i}T$, T is the temperature. This defined transition amplitude A_t can be calculated by using the path integral method [56] for periodic instanton. Then, we can find the decay rate Γ by comparing the defined amplitude A_t in Eq. (17) with the calculated amplitude A_t in following Eq. (18).

All instantons were totally independent in the dilute gas approximation, the total transition amplitude A_t is summate over all the instanton contributions

$$A_t = \mathrm{e}^{-2E\beta - \mathrm{i}\frac{\beta}{\mathcal{K}_1(k')}\sqrt{\frac{8\pi^2 U_d(x,y)\cos\theta_0(z_1 - z_3)}{3m\lambda^2}}\mathrm{e}^{-\Omega}} \tag{18}$$

where

$$\begin{aligned} \Omega &= [(1-k^2)(k^2-2)\mathcal{K}_1(k) + 2(k^4 - k^2 + 1)\mathcal{K}_2(k)] \\ &\quad \times \frac{64k^4}{15\hbar}\sqrt{\frac{2\pi m}{3\lambda}U_d(x,y)\cos\theta_0}(z_1 - z_3)^{\frac{5}{2}} \end{aligned} \tag{19}$$

here $\mathcal{K}_1(k)$ and $\mathcal{K}_2(k)$ are the complete first and second kinds elliptic integrals.

Generally, by comparing calculated amplitude A_t in Eq. (18) with defined amplitude A in Eq. (17), we find that the decay rate at finite energy E can be written as

$$\Gamma = \frac{\omega_E}{\hbar\mathcal{K}_1(k')}\mathrm{e}^{-\Omega} \tag{20}$$

where $\omega_E = \sqrt{2(z_1 - z_3)/3}\omega_0$ is the frequency depend on energy. It describes the frequency of small oscillations $\omega_0 = \sqrt{16\pi^2 U_d(x,y)\cos\theta_0/(m\lambda^2)}$ around the metastable minimum. This compact formula is valid for the entire region of energy $0 < E < U_{max}$, here

$$U_{max} = U_0 + \frac{1}{6}U_d(x,y)\cos\theta_0\cot^2\theta_0 \tag{21}$$

It can be used to applied for any excited states from the bottom to the top of the well. For energies far below the barrier maximum $E \ll U_{max}$, the decay rate Γ_n of

nth low excited state can be evaluated by introducing the harmonic approximation $E_n = n\hbar\omega_0 + E_0$,

$$\Gamma_n = \frac{1}{n!}\left(\frac{432U_{max}}{\hbar\omega_0}\right)^n \Gamma_0 \tag{22}$$

When $n = 0$, Γ_n reduces to Γ_0 of the metastable ground state with energy E_0,

$$\Gamma_0 = 12\omega_0\sqrt{3U_{max}/(2\pi\hbar\omega_0)}\,\mathrm{e}^{-\frac{36U_{max}}{5\hbar\omega_0}} \tag{23}$$

The decay rate depends on the depth of the well. The tunneling rate from the well could be controlled by adjusting the depth of the optical wells $U_l(x, y)$, so that it was slow enough to observe many of the temporally modulated signal periods directly before the traps were depleted, but fast enough to observe atoms leaving the traps. By lowering the well depths, the tunneling rate could be increased which producing fewer pulses with more atoms per pulse. This interesting phenomenon has been observed in experiments. We also find that the Landau–Zener tunneling rate will not depend on the depth of the well, and it is constant in experiments [51, 52].

Figure 5 shows the decay rates Γ_0 of Wannier–Stark regime and $\Gamma_{\rm LZ}$ of Landau–Zener regime as a function of acceleration a for sodium atoms with experimental parameters: $U_0/h = 72$ kHz, $k_l = 1.37\times10^7$ m^{-1}, where $\Gamma_{\rm LZ} = \frac{ma}{2\hbar k_l}\mathrm{e}^{-\frac{a_c}{a}}$, $a_c = \pi E_{gap}^2/(4\hbar^2 k_l)$ is a critical acceleration, $E_{gap}/h = 70$ kHz is the energy gap between the first and second bands [25]. We can find that the system is in the Landau–Zener tunneling regime for $a < a_{eq}$, whereas for $a > a_{eq}$ the system shifts to the Wannier–Stark regime, where a_{eq} is the acceleration when $\Gamma_0 = \Gamma_{\rm LZ}$. It is note that $a_{eq} < a_c$. For sodium atoms with previous experimental parameters, $a_{eq} = 1.064\times10^4$ m/s^2 $< a_c = 1.109\times10^4$ m/s^2.

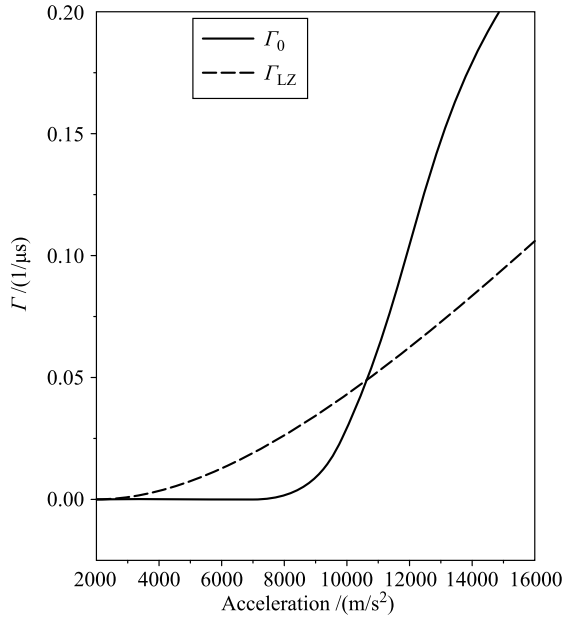

Fig. 5 The acceleration dependence of the decay rate Γ_0 for sodium atoms of Wannier–Stark regime and $\Gamma_{\rm LZ}$ of Landau–Zener regime with experimental parameters: $V_0/h = 72$ kHz, $k_l = 1.37\times10^7$ m^{-1}, where $\Gamma_{\rm LZ} = \frac{ma}{2\hbar k_l}\mathrm{e}^{-a_c/a}$, $a_c = \pi E_{gap}^2/(4\hbar^2 k_l)$ is a critical acceleration, $E_{gap}/h = 70$ kHz is the energy gap between the first and second bands.

Comparing the decay rate Γ_0 of the Wannier–Stark regime with $\Gamma_{\rm LZ}$ of the Landau–Zener regime for experiments [51, 52] is very interesting. With Yale experimental parameters for ^{87}Rb atoms, we find that $\Gamma_0 = 12.26\times10^3$ s^{-1}, $\Gamma_{\rm LZ} = 12.37$ s^{-1}. The Landau–Zener regime lifetime is 88 ms, and it is very close to lifetime 50 ms observed in the Yale experiment [51]. For ^{87}Rb atoms with Istituto Nazionale di Fisica della Materia(INFM) experimental parameters, $\Gamma_0 = 2.36\times10^3$ s^{-1} and $\Gamma_{\rm LZ} = 2.6$ s^{-1}. The corresponding Landau–Zener regime lifetime is $0.39s$, and it is very close to the lifetime 0.3 s observed in the INFM experiment [52]. Atoms in the Wannier–Stark regime decay faster 1000 times than those in the Landau–Zener regime in both cases.

3.2 Temperature dependence

The temperature dependence of the decay rate can be obtained by taking a statistical average of the decay rates of different states,

$$\Gamma(T) = \Gamma_0(1-\mathrm{e}^{-\hbar\omega_0/(k_{\rm B}T)})\mathrm{e}^{\frac{432U_{max}}{\hbar\omega_0}\mathrm{e}^{-\hbar\omega_0/(k_{\rm B}T)}} \tag{24}$$

where $k_{\rm B}$ is the Boltzmann constant. For rudibium atoms with experimental parameters: $V_0/h = 72$ kHz, $k_l = 1.37\times10^7$ m^{-1}, $a = 8\times10^3$ m/s^2, Fig. 6 shows three obvious regions with different behavior for $\Gamma(T)$. The decay is purely thermally activated and exhibits the expected

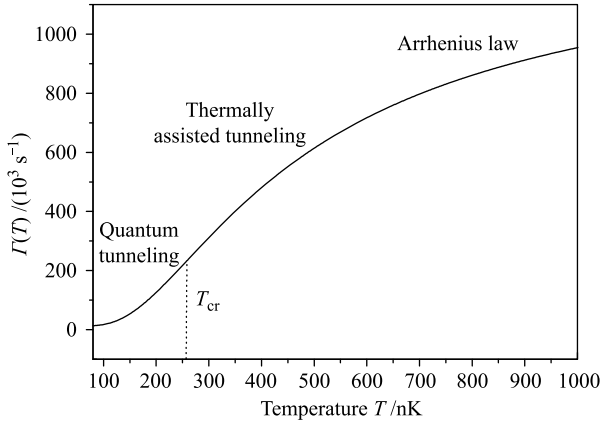

Fig. 6 The temperature dependence of the decay rate $\Gamma(T)$ for ^{87}Rb atoms with Yale experimental parameters $\lambda = 850$ nm, $U_d(x, y) = 2.1E_R$, where $E_R = 2\pi^2\hbar^2/(m\lambda^2)$ is the recoil energy. Reproduced from Ref. [49], Copyright © 2002 American Physical Society.

Arrhenius law behavior at high temperature [53], $\Gamma_{AR} = \frac{\omega_0}{2\pi} e^{-\frac{U_{max}}{k_B T}}$. At intermediate temperature, "thermally assisted" tunneling was observed, in which the atom is thermally excited to a excited quantum states and the decay then proceeds from these states by quantum tunneling. And at a still lower temperature, the regime of pure quantum tunneling come out from the trapped ground state, which is controlled by the "vacuum" instanton trajectory. Thus we can define $T_c r = \frac{\hbar\omega_0}{2\pi k_B}$ as the "crossover" temperature, below which quantum tunneling dominates. The decay rate will increase with temperature raising when above $T_c r$ and is independent with temperature when below $T_c r$.

To make clear of the meaning of $\Gamma(T)$, we assume that the population with an initial thermal distribution of the atoms decay as

$$N(t) = \frac{N_0}{Z_0} \sum_n e^{-\Gamma_n t - \frac{E_n}{k_B T}} \tag{25}$$

where N_0 is the initial population of trapped atoms. $N(t)$ does not decay exponentially itself because it is a sum of exponential decay factors, i.e., if we plot $\log N(t)$ as a function of time, it is not a straight line. Since there is not a single slope, it cannot be assigned a single decay rate. At long times, with the corresponding rate given by Γ_0, the curve approaches a straight line, in other words, the slowest channel dominates the long time behavior. As a matter of fact, the slope at time $t = 0$ corresponds to the rate of $\Gamma(T)$ as calculated, that is to say, $\Gamma(T)$ is simply the initial rate of decay of the population.

If there is no thermalization of the population during decay, the above discussion is valid, which is a situation that the experimentalist can realize. On the other side, such that thermalization can be established in a time t_c by intentionally introducing intra-well transitions between the different levels. In this case, if t_c compared to $1/\Gamma(T)$ is short, the rate will decay at $\Gamma(T)$ at all times. If it is larger than $1/\Gamma(T)$, the rate will decay initially non-exponentially until time t_c, and after t_c the rate will decay at $\Gamma(T')$, where T' is any temperature below T. Due to the initial decay, there will be a cool down of the population.

3.3 Experimental observation

The phenomenon of the Wannier–Stark intraband transitions in lattice potentials which been studied theoretically have been demonstrated experimentally for the first time by Ivanov *et al.* in 2008. In their experiment (see Fig. 4), the lattice potential has the form [54]:

$$U(z,t) = mgz + \frac{U_0}{2}\cos\{2k_L[z - z_0\cos(2\pi\nu_m t)]\} \tag{26}$$

where the lattice depth is U_0, the gravity potential is mgz, the optical-lattice wave vector is k_L, the phase-modulation amplitude and frequency are z_0 and ν_m respectively.

The experiment was started by cooling and trapping about 2×10^7 ^{88}Sr atoms at 3 mK which in a magneto-optical trap operating on the resonance line of $^1S_0 - ^1P_1$ at 461 nm. Then by a second cooling stage in a red magneto-optical trap operating on the $^1S_0 - ^3P_1$ narrow transition at 689 nm, the temperature is further reduced and finally obtain $\sim 5 \times 10^5$ atoms at 1 μK. This preparation stage takes about 2.5 s. In 150 μs, the red magneto-optical trap was switched off and a one-dimensional optical lattice which was originated by a single mode frequency doubled Nd:YVO_4 laser was adiabatically switched on. The wave length of the beam $\lambda_L = 532$ nm and it was vertically aligned and retro-reflected by a mirror producing a standing wave with a half-wavelength $\lambda_L/2 = 266$ nm. The corresponding photon recoil energy was chosen as $E_R = h^2/(2m\lambda_L^2) = k_B \times 381$ nK, and the maximum lattice depth was chosen as 20 E_R. The phase of the lattice potential can be modulated by mounting a piezo-eletric transducer (PZT) on the retro-reflecting mirror, and the PZT was driven at frequency ν_m by a synthesized frequency generator.

How can the intraband transitions between Wannier–Stark levels observed experimentally? For Wannier–Stark tunneling give rise to coherent delocalization effects, this can be observed through a coherent ballistic expansion of the atomic wave packet which well-localized initially. Wannier–Stark intraband tunneling is not affected by typical decoherence mechanisms which usually occurring in the Landau–Zener intraband case. Line broadening due to the transverse profile of the lattice potential is one of the most obvious different. The atomic species ^{88}Sr remarkably robust against decoherence processes, which capacitate us to observe Wannier–Stark tunneling up to five neighboring levels, corresponding to driven tunneling across five neighboring sites coherently. Thus the resonance spectra exhibit Fourier-limited widths over excitation times of the order of seconds owing to such a quantum robustness.

A generalized two-level system can describe the dynamics of tunneling between two distinct Wannier–Stark levels, on the other, the coherent transitions over a large number of lattice periods can describe the line broadening. This hypothesis can be verified by studying the response of the system at different driving frequencies. First of all, the shape of the resonance will be discussed when the modulation close to the Bloch frequency $\nu_m \simeq \nu_B$. A typical data set of the atomic extent for different modulation frequencies are shown in the inset of

Fig. 7, while the potential depth, the excitation time and the amplitude of modulation keeping constant. The data points are well fitted with the following function:

$$\eta(\nu_m, t) = \sqrt{\eta_0^2 + v_n^2 t^2 \mathrm{sinc}(\frac{\nu_m - n\nu_B}{\Gamma})^2} \quad (27)$$

where $\mathrm{sinc}(x)$ is the resonance function $\frac{\sin x}{x}$ for a two-level transition probability and accounts for the resonance term in the tunneling rate, Γ represents the resonance half width at half maximum which will be measured for varying excitation times T when modulating at a frequency close to ν_B. The results are shown in Fig. 7, where the linewidth of the resonance for an excitation time varying between 50 ms to 2 s. As expected from the ideal two-level system, the accordance of the data with the hyperbola $1/(\pi T)$ forecast that the resonance linewidth is purely Fourier limited. Under their experimental conditions, for increasing the sensitivity of force measurements with submillimeter spatial resolution, coherent intraband Wannier–Stark tunneling turns out to be quite practical. More details see Ref. [54].

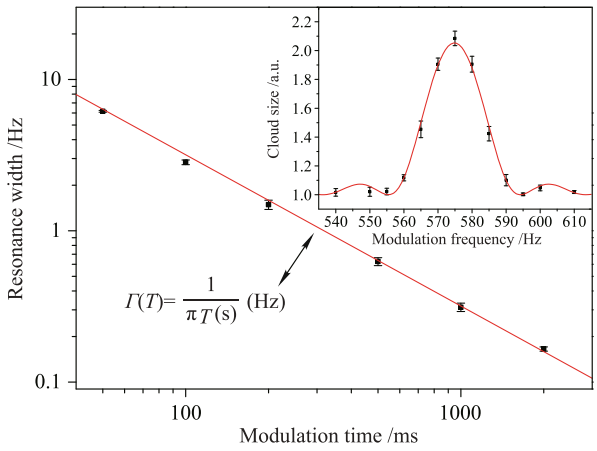

Fig. 7 Resonance width as function of the modulation time T. The resonance is probed in the region $\nu_m \simeq \nu_B$. The solid line (*red line*) is the hyperbola $(\pi T)^{-1}$ expected from a Fourier-limited resonance width in a two-level system. Inset: resonance spectrum for 50 ms excitation time. The fitting function is of the form of Eq. (27). Reproduced from Ref. [54], Copyright © 2008 American Physical Society.

4 Quantum tunnneling in two linked microcavities

In this part, we explore the Josephson effects of photons of a many-body optical system with strongly interactions where the polaritons condense into a superfluid quantum phase [57]. The wave function of this superfluid quantum phase is a superposition of the coherent states of photons and two-level atoms [58]. The order parameter of photon wave-funtion can describe the superfluid phase by an effective field theory when the freedom of the atom polarization are integrated out [64]. These coherent photons can serve as good candidates for the quantum simulations of the correlation effects since they are novel quasiparticles that are self-interacting and behave like massive bosons in condensed matter physics.

4.1 The Hamiltonian and excitations

By measuring the chemical potential-current relation of the ac and dc Josephson effects in real experiments, the striking signatures of the Josephson effects are demonstrated [59]. But in neutral systems such as atomic BECs, it is very difficult to implement the chemical potential-current relation for the external circuits and current sources are absent [60]. Here an optical correlation system has been set up. As shown in Fig. 8, the system contained two fibre-based Fabry–Perot (FFP) or ultrahigh-finesse optical cavities [61, 63], which can achieve a strong coupling regime with a small rate of decay of the cavity field κ and large single-atom peak coupling rate j_0. By moving the atoms in a modulated local atom-field, a time-dependent coupling between the moving atoms and cavity photons can be realized, thus a biased photonic current could be applied. This technique provides a practical way to explore the Josephson effects of photons for the first time, which play an important role for understanding the temporal interference of coherent photons.

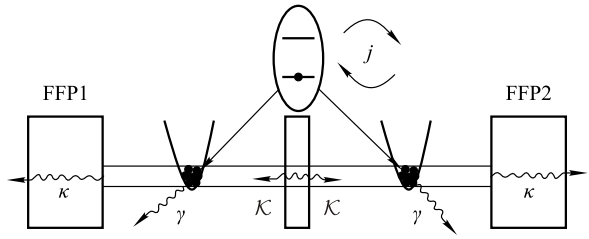

Fig. 8 Experimental set-up. Two fibre-based Fabry–Perot (FFP) cavities are linked with a intercavity tunneling amplitude $\mathcal{K}$. Each cavity contains N^{a} two-level ^{87}Rb atoms trapped by an external magnetic potential or dipole beam. g is the coherent coupling rate between an individual atom and the cavity field, γ and κ are the dissipation rate of the atomic spontaneous emission and the cavity field itself. Reproduced from Ref. [57], Copyright © 2009 American Physical Society.

The two cavities contains $N^{\mathrm{a}} = 10^4$ two-level ^{87}Rb atoms which trapped by an external magnetic potential or dipole beam respectively and are linked with the intercavity tunneling amplitude $\mathcal{K}$. The relevant parameters were chosen as $j_0/(2\pi) = 215$ MHz [63] and $(\kappa, \gamma)/(2\pi) = (1.3, 3.0)$ MHz [61]. In Fig. 9(a), in order to increase the atomic confinement and gain control over the coupling rate, a far-detuned optical lattice was switched on, here the period of the overlap between the

cavity mode and optical lattice is 6.4 μm [61]. A tunable coupling rate can be realized by moving the ultracold atoms within the cavity, which is crucial for the realization of the d.c. Josephson effects of photons experimentally. The modulated local atom-field coupling rate $j(x)$ is shown in Fig. 9(b), where

$$j^2(x) = \int \frac{\rho(\boldsymbol{r})}{N^{\rm a}} |g_0 \cos(2\pi x/\lambda_{\rm c}) \exp(-r_\perp^2/w^2)|^2 {\rm d}\boldsymbol{r}$$

with $\lambda_{\rm c}$ and w being the wave-length and mode radius.

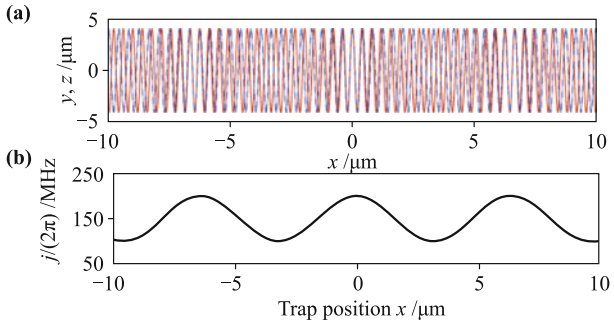

Fig. 9 Control of the coupling along the resonator axis. **(a)** The atoms are placed at a position x along the cavity axis, and are loaded into the optical lattice. The cavity mode ($\lambda_{\rm c} = 780$ nm) and far-detuned optical lattice ($\lambda_{\rm L} = 830$ nm) standing waves in each cavity have a variable overlap with 6.4 μm period. **(b)** The loaded atoms show a strongly modulated coupling depending on the local overlap between lattice and cavity mode. Reproduced from Ref. [57], Copyright © 2009 American Physical Society.

In the rotating-wave approximation, the Hamiltonian of this system with Josephson coupled atom-field interaction can be described by a combination of the Dicke Hamiltonian [62] with photon tunneling between two weakly linked microcavities. The dynamics of the full system is determined by the following Hamiltonian

$$\hat{H} = \sum_{i=1,2} \hat{H}_i + \mathcal{K}(\hat{p}_1^\dagger \hat{p}_2 + \hat{p}_1 \hat{p}_2^\dagger) \tag{28}$$

$$\hat{H}_i = \omega_{\rm c} \hat{p}_i^\dagger \hat{p}_i + \sum_{j=1}^{N^{\rm a}} \frac{\omega_{\rm a}}{2} (\hat{b}_{i,j}^\dagger \hat{b}_{i,j} - \hat{a}_{i,j}^\dagger \hat{a}_{i,j}) + j_i (\hat{b}_{i,j}^\dagger \hat{a}_{i,j} \hat{p}_i + \hat{p}_i^\dagger \hat{a}_{i,j}^\dagger \hat{b}_{i,j}) \tag{29}$$

where $\omega_{\rm a}$ and $\omega_{\rm c}$ are the atom and cavity resonance frequencies with the detuning $\Delta_{\rm c} = \omega_{\rm c} - \omega_{\rm a}$. $\hat{a}_{i,j}$ and $\hat{b}_{i,j}$ are fermion operators, which are satisfy the single-occupancy constraint [64] and naturally associated with the lower and upper levels of each atom; $\hat{p}_i^\dagger(\hat{p}_i)$ is the single-mode creation (annihilation) operator of the photons in each cavity.

$$\mathcal{K} = 2\omega_{\rm c} \int {\rm d}\boldsymbol{r} (\epsilon_i(\boldsymbol{r}) - \epsilon(\boldsymbol{r})) w_1^*(\boldsymbol{r}) w_2(\boldsymbol{r}) \tag{30}$$

represents the intercavity tunneling amplitude [65], where $w_i(\boldsymbol{r})$ and $\epsilon_i(\boldsymbol{r})$ are the eigenmode of an individual single cavity and the dielectric function, $\epsilon(\boldsymbol{r})$ is the dielectric function of the coupled cavities, and the modulated local atom-field coupling rate is $j_i(x) \simeq 2\pi \times [50\cos(2\pi x/6.4) + 150]$ MHz.

The excitations of the atom-cavity system will be analyzed with the Hamiltonian (29) in the grand-canonical ensemble

$$\tilde{\hat{H}}_i = \hat{H}_i - \mu_i \hat{N}_i^{\rm e} \tag{31}$$

with

$$\hat{N}_i^{\rm e} = \sum_{j=1}^{N^{\rm a}} \frac{1}{2} (\hat{b}_{i,j}^\dagger \hat{b}_{i,j} - \hat{a}_{i,j}^\dagger \hat{a}_{i,j} + 1) + \hat{p}_i^\dagger \hat{p}_i \tag{32}$$

which fixed the total number of excitations. An effective action for photons is the first step to study the excitations of the system, and it will be arrived by using the coherent state functional integral representation for the partition function [64, 58] with single-occupancy constraint $\hat{a}_{i,j}^\dagger \hat{a}_{i,j} + \hat{b}_{i,j}^\dagger \hat{b}_{i,j} = 1$ and integrating over the fermion fields,

$$S_{\rm e}[\varphi_i] = \int_0^\beta {\rm d}\tau \varphi_i^* (\partial_\tau + \tilde{\omega}_{\rm c}^i) \varphi_i - \mu_i N^{\rm a}/2 - N^{\rm a} {\rm Tr} \ln \begin{pmatrix} \partial_\tau + \tilde{\varepsilon}_i & j_i \varphi_i / \sqrt{N^{\rm a}} \\ j_i \varphi_i^* / \sqrt{N^{\rm a}} & \partial_\tau - \tilde{\varepsilon}_i \end{pmatrix} \tag{33}$$

here $\tilde{\omega}_{\rm c}^i = \omega_{\rm c} - \mu_i$ and $\tilde{\varepsilon}_i = (\omega_{\rm a} - \mu_i)/2$. Then by making the static assumption $\varphi_i(\tau) = \Psi_i$, the free energy is written as

$$F_i = \ln[2\cosh(\frac{1}{2}\beta \mathcal{E}_i))]/\beta + \tilde{\omega}_{\rm c}^i |\Psi_i|^2 - \mu_i N^{\rm a}/2 \tag{34}$$

with $\mathcal{E}_i = \sqrt{\tilde{\varepsilon}_i^2 + j_i^2 |\Psi_i|^2}$.

The saddle condition $\partial F_i / \partial \Psi_i^* = 0$ combined with the excitation density constraint equation

$$\rho_i^{\rm e} = \frac{1}{\beta N^{\rm a}} \frac{\partial F_i}{\partial \mu_i} \tag{35}$$

determined the mean-field equations of a polariton condensate, which read

$$\tilde{\omega}_{\rm c}^i \Psi_i = j_i^2 N^{\rm a} \frac{\Psi_i}{2\mathcal{E}_i}$$
$$\rho_i^{\rm e} - \frac{1}{2} = \frac{|\Psi_i|^2}{N^{\rm a}} - \frac{\tilde{\varepsilon}_i}{2\mathcal{E}_i} \tag{36}$$

Here we only considered the zero-temperature excitations of the system with the ground state energy of the Hamiltonian (29) given by $E_i = \tilde{\omega}_{\rm c}^i |\Psi_i|^2 - N^{\rm a}\mathcal{E}_i - \mu_i N^{\rm a}/2$ by letting $\beta \to \infty$.

The coherent field amplitude Ψ of the system and the chemical potential μ are dependent on the excita-

tion density ρ^{e} and detuning Δ_{c} when the atoms are placed at a position of the cavity with a fixed coupling rate j. From the inset of Fig. 10 we can see that there exists an important feature of the above equations (36): the photon occupancy density $\rho = |\Psi|^2/N^{\mathrm{a}}$ is linearly dependent on the excitation density approximately for the low excitation density ($\rho^{\mathrm{e}} < 0.5$) and the atomic resonance ($\Delta_{\mathrm{c}} = 0$). When the photonic tunneling between two cavities was considered, this linear relation will be beneficially for it can keep constant the total number of the coherent photons of two weakly linked polariton condensates.

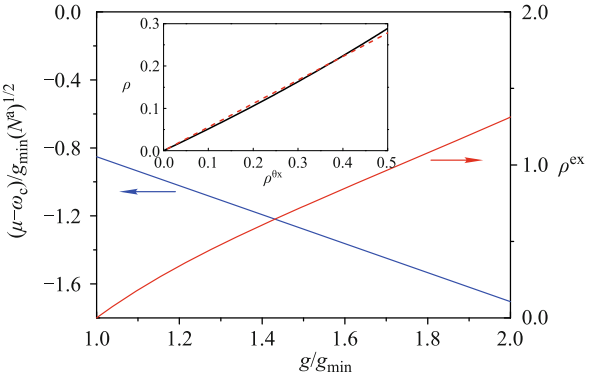

Fig. 10 Excitations of a polariton condensate. This diagram shows the dependence of excitation density ρ^{e} on the coupling rate j for chemical potential $(\mu - \omega_{\mathrm{c}})/j_{\min}\sqrt{N^{\mathrm{a}}} = -1$ (*red line*), and the chemical potential as a function of g for the excitation density $\rho^{\mathrm{e}} = 0.3$ (*blue line*). Inset shows the photon occupancy density ρ^p as a function of the excitation density ρ^{e} for atomic resonance ($\Delta_{\mathrm{c}} = 0$), where the red dashed line is the linear fitting. Reproduced from Ref. [57], Copyright © 2009 American Physical Society.

Besides, see Fig. 8(b), a far-detuned optical lattice have been switched on to modulate the atom-field coupling rate. The atoms moving along the cavity axis can feel a tunable coupling rate $j(x)$, resulting in a variable excitations in the atom-cavity system. As shown in Fig. 10, the chemical potential as a function of j for $\rho^{\mathrm{e}} = 0.3$, and the excitation density ρ^{e} depend on the coupling rate j for $(\mu-\omega_c)/j_{\min}\sqrt{N^{\mathrm{a}}} = -1$. The conclusion is that the tunable coupling rate determined the excitations, which enables an investigation of the Josephson effects of photons.

4.2 The ac and dc Josephson effects of photons

The two cavities are initially tuned to atomic resonance and the polariton condensates are excited in equilibrium with low excitation density. Then the macroscopic wave function of the system can be described as

$$|\Psi(t)\rangle = \Psi_1(t)|1\rangle + \Psi_2(t)|2\rangle \tag{37}$$

with

$$\Psi_i(t) = \sqrt{N_i^p(t)}\mathrm{e}^{\mathrm{i}\theta_i^p(t)} \tag{38}$$

being the complex amplitudes, and $|i\rangle$ being the two base states for each polariton condensate [66, 67]. Although the photon occupations $N_i^p(t)$ and phases $\theta_i^p(t)$ are time-dependent, the total amount of the coherent photons $N^p = N_1^p + N_2^p$ is a constant. The ground state energy of each atom-cavity system can be expand to the second order of the coherent photon occupancy density for low density excitations. Then the effective nonlinear Schrödinger equation will be get which can describe the dynamics of the coherent tunneling of photons approximately

$$\mathrm{i}\hbar\frac{\partial|\Psi(t)\rangle}{\partial t} \simeq [\sum_i (E_i^0 + U_i|\Psi_i|^2)|i\rangle\langle i| + \mathcal{K}(|1\rangle\langle 2| + |2\rangle\langle 1|)]|\Psi(t)\rangle \tag{39}$$

where

$$U_i = j_i/(16\sqrt{N^{\mathrm{a}}}\mathcal{U}_i^3) \tag{40}$$

are the effective self-interactions of photons induced by the coupling between the atoms and the photons and

$$E_i^0 = \omega_{\mathrm{c}} - \mu_i - j_i/(4\mathcal{U}_i) \tag{41}$$

are the zero-point energies in each cavity with $\mathcal{U}_i$ is the dimensionless chemical potential which defined as

$$\mathcal{U}_i = (\omega_{\mathrm{c}} - \mu_i)/(j_i\sqrt{N^{\mathrm{a}}}) \tag{42}$$

Then the equations of motion for the relative population $\delta(t)$ and relative phase $\phi(t)$ can be obtained from the above equation (39), which read

$$\hbar\dot{\delta}(t) = (2E_{\mathrm{J}}/N^p)\sqrt{1-\delta^2(t)}\sin\phi(t) \tag{43}$$

$$\hbar\dot{\phi}(t) = \frac{2E_{\mathrm{J}}\delta(t)}{N^p\sqrt{1-\delta^2(t)}}\cos\phi(t) + \frac{NE_{\mathrm{c}}}{2}\delta(t) + Fl_x(t) \tag{44}$$

where $E_{\mathrm{c}} = U_1 + U_2$ is the capacitive energy which is almost a constant and $E_{\mathrm{J}} = N^p\mathcal{K}$ is the Josephson coupling energy. The motion of the atoms in one of the cavities can be described by $l_x(t)$, and the average force on single atoms exerted by the external trap is

$$F = \sqrt{N^{\mathrm{a}}}[\rho^{\mathrm{e}}/(2\mathcal{U}^3) - 1/(2\mathcal{U})]\frac{\mathrm{d}j}{\mathrm{d}x} \tag{45}$$

which generates the chemical potential difference $Fl_x(t)$ between the two cavities. Here, both of the condensates are excited with the same dimensionless chemical potential $\mathcal{U}$ at the beginning in each cavity.

confined to the Josephson regime ($E_{\mathrm{c}} \gg E_{\mathrm{J}}$), and just consider a small population imbalance ($\delta \ll 1$). In this case, the critical current of photons was given by $\omega_{\mathrm{J}} = 2E_{\mathrm{J}}/(\hbar N^p)$ and Eq. (43) is reduced to the atomic

current-phase relation $\dot{\delta} \simeq \omega_J \sin\phi$. Then by combining with Eq. (44), we get the driven pendulum phase equation

$$\ddot{\phi} = \omega_p^2(\sin\phi + v/v_c) \tag{46}$$

where $v_c = \hbar\omega_p^2/F$ is the critical velocity and $\omega_p = \sqrt{E_J E_c}/\hbar$ is the Josephson plasma frequency. Furthermore, the phase evolution equation $\dot{\phi} = -\Delta\mu/\hbar$ applies with the chemical potential difference $\Delta\mu = \mu_1 - \mu_2$ for the condensates in the Josephson regime. Then an analogous superconducting circuit [60] will be derived,

$$\omega_J \sin\phi + \sigma\Delta\mu + \Delta\dot{\mu}/(N^p E_c/2) = \dot{\delta}_{equil} \tag{47}$$

where σ is the conductance due to the noncoherent photons, which is negligible during the characteristic time scale of the cavity coherent process. δ_{equil} is the equilibrium value of the relative population and $\dot{\delta}_{equil} = \omega_J v/v_c$ is the applied current of photons bias. Finally, the chemical potential difference is associated with the population imbalance $\Delta\mu = \frac{N^p E_c}{2}(\delta - \delta_{equil})$. In experiments, this relation can be used to measure the chemical potential difference between two cavity polariton condensates.

As shown in Fig. 11, the chemical potential-current relation was performed by solving Eqs. (43) and (44) numerically. At the very beginning, both the polariton condensates are excited at a density $\rho^e = 0.3$ and the atoms in each cavity are positioned at $x = 1.6$ μm. $E_c N^p/\hbar = 7.06$ ns^{-1} and $E_J/(\hbar N^p) = 6.29 \times 10^{-4}$ ns^{-1} are the corresponding value of the energy parameters with the intercavity tunneling amplitude $\mathcal{K} = 2\pi \times 0.1$ MHz. Then in one of the cavities, the atoms are moved at a constant velocity with the average force $F = 6.6$ ns$^{-1}\cdot$μm^{-1}, and at $t_f = 200$ ns the population imbalance between two cavities will be finally observed.

In Fig. 11(c), the dependence of the chemical potential difference and the relative population on the velocity of the moving optical lattice are shown, at $v_c = 0.48$ μm/μs which exhibits a sharp transition. When the velocity of the moving lattices below the critical velocity, the system takes an averaged constant phase difference between two condensates with applied a finite photonic current source $\dot{\delta}_{equil}$, see Fig. 11(a). The chemical potential difference is directly proportional to the time average of $\dot{\phi}$, that is to say, $\Delta\mu/\hbar = \frac{1}{t_f}\int_0^{t_f}\dot{\phi}dt$, in this case, it is locked around zero. Thus a coherent photonic current $\dot{\delta} = \dot{\delta}_{equil}$ flows constantly through the cavities and finally achieve a finite population imbalance. This is the d.c. photonic Josephson effect, which can be measured in cavity experiment. Additionally, $\dot{\delta}_{equil}$ exceeds the critical photonic current ω_J when $v > v_c$, as shown in Fig. 11(b), the population imbalance remains on a low average value and the relative phase starts running. This lead to some photonic

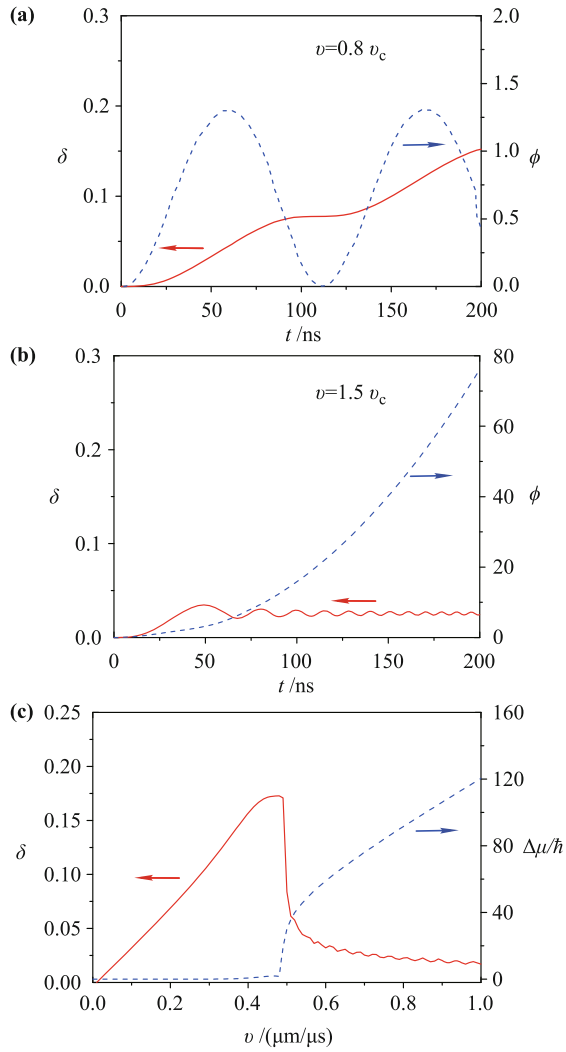

Fig. 11 The chemical potential-current relation in the polariton condensates. **(a)** and **(b)** Time evolution of the relative population (*solid line*) and phase (*dashed line*) for $v = 0.8v_c$ (a) and $v = 1.5v_c$ (b). **(c)** Dependence of the relative population (*solid line*) and the chemical potential difference (*dashed line*) on the velocity of the moving optical lattice. This diagram shows that there exists a sharp transition with the critical velocity $v_c = 0.48$ μm/μs. Reproduced from Ref. [57], Copyright © 2009 American Physical Society.

current flows through the capacitive paths, which resulting in a finite chemical potential difference $\Delta\mu$. The ac Josephson effect of photons can be observed in this case, that is to say the oscillations of population difference between the two cavities.

By measuring the coherent photons transmitted from each cavity with a standard photon counting system, the dc and ac Josephson effects of photons can be observed experimentally. In the atom-cavity system, the dynamics of the atom-cavity system is quantum dissipative with the atom-field interaction is in the strong coupling regime [68]. The cavity photon lifetime $\tau_\kappa = 2\pi/\kappa \sim 754$ ns and atom spontaneous emission lifetime $\tau_\gamma = 2\pi/\gamma \sim 330$

ns determined the typical time scales of the dissipations. Here, the operation time was chosen at $t_f = 200$ ns. This is corresponds to a couple of plasma oscillations with period $\tau_p = 2\pi/\omega_p \sim 100$ ns within the above time scales.

The motion of the atoms is another aspect of our proposal that should be considered. The atoms are confined in a single lattice site by ramping up a tight optical lattice in each cavity. The kinetic energy increasing rate of the atoms should be smaller than the harmonic frequency of the optical lattice when the external trap moved the atoms in one of the cavities, thus the atoms could be adiabatically moved. Moreover, the Bose–Einstein condensates of the atoms should coupled to the cavities as shown in the recent experiment [61] to confine the atoms in a single lattice site. As shown in the supplementary notes of Ref. [61], the kinetic energy of the atoms then can be neglected, which is valid for the wide line condition $E_{\rm rec} \ll \hbar\Gamma$. Further, it was found that the energy spectrum of the excitation will not affected by heating of BECs.

5 Conclusions and perspective

In summary, we review our theoretical advances in quantum tunneling of Bose–Einstein condensates by proposing an experimental protocol to realize the so called non-Abelian Josephson effect in spin-2 Bose system which involves non-Abelian symmetry in the first place. We find that the frequencies of pseudo Goldstone modes relate to both the coupling parameter and the interacting strengthes, which is a nonlinear effect. These results are of particular significance for exploring the novel features of the non-Abelian Josephson effect which are very distinct from the Abelian case. Then we investigate the quantum tunneling in optical lattices under gravity, and we finally get the pure quantum tunneling at low temperatures. At last, we show how to implement the quantum tunneling of coherent photons between two cavity polariton condensates. Such protocol allow us to observe the dc and ac Josephson effect of photons directly, which is of great help to explore new phenomena of ultracold atoms and cavity quantum electrodynamics. Additionally, our proposal may be useful to realize quantum interference devices in the future.

Acknowledgements This work was supported by the National Key Basic Research Special Foundation of China (Grant Nos. 2011CB921502, 2012CB821305, 2009CB930701, and 2010CB922904), the National Natural Science Foundation of China (Grant Nos. 10934010, 11228409, and 61227902), and the National Natural Science Foundation of China-The Research Grants Council (Grant Nos. 11061160490 and 1386-N-HKU748/10).

References

1. J. R. Gordon, C. Teague, R. A. Serway, and Chris Vuille, College Physics, Vol. 2, Brooks Cole Publishing Company
2. J. R. Taylor, C. D. Zafirators, and M. A. Dumbson, Modern Physics for scientists and engineers, Pearson Prentice Hall, 2004: 234
3. M. Razavy, Quantum Theory of Tunneling, Singapore: World Scientific, 2003: 4, 462
4. G. Nimtz and A. Haibel, Zero Time Space, Wiley-VCH, 2008: 1
5. B. Xia, W. Hai, and G. Chong, Stability and chaotic behavior of a two-component Bose–Einstein condensate, *Phys. Lett. A*, 2006, 351(3): 136
6. Q. Zhang, P. Hanggi, and J. Gong, Two-mode Bose–Einstein condensate in a high-frequency driving field that directly couples the two modes, *Phys. Rev. A*, 2008, 77(5): 053607
7. N. Tsukada, M. Gotoda, Y. Nomura, and T. Isu, Laser-assisted coherent atomic tunneling between two trapped Bose–Einstein condensates, *Phys. Rev. A*, 1999, 59(5): 3862
8. H. L. Zheng and Qiang Gu, Dynamics of Bose–Einstein condensates in a one-dimensional optical lattice with doublewell potential, *Front. Phys.*, 2013, DOI: 10.1007/s11467-013-0321-0
9. C. E. Creffield, Coherent control of self-trapping of cold bosonic atoms, *Phys. Rev. A*, 2007, 75(3): 031607
10. C. Weiss and N. Teichmann, Differences between mean-field dynamics and N-particle quantum dynamics as a signature of entanglement, *Phys. Rev. Lett.*, 2008, 100(14): 140408
11. A. Eckardt, T. Jinasundera, C. Weiss, and M. Holthaus, Analog of photon-assisted tunneling in a Bose–Einstein condensate, *Phys. Rev. Lett.*, 2005, 95(20): 200401
12. T. Jinasundera, C. Weiss, and M. Holthaus, Manyparticle tunnelling in a driven bosonic Josephson junction, *Chem. Phys.*, 2006, 322(1–2): 118
13. N. Teichmann, M. Esmann, and C. Weiss, Fractional photon-assisted tunneling for Bose–Einstein condensates in a double well, *Phys. Rev. A*, 2009, 79(6): 063620
14. M. Holthaus, Towards coherent control of a Bose–Einstein condensate in a double well, *Phys. Rev. A*, 2001, 64(1): 011601(R)
15. S. Kohler and F. Sols, Chemical potential standard for atomic Bose–Einstein condensates, *New J. Phys.*, 2003, 5: 94
16. X. F. Zhang, X. H. Hu, D. S. Wang, X. X. Liu, and W. M. Liu, Dynamics of Bose–Einstein condensates near Feshbach resonance in external potential, *Front. Phys.*, 2011, 6(1): 46
17. G. F. Wang, L. B. Fu, and J. Liu, Periodic modulation effect on self-trapping of two weakly coupled Bose–Einstein condensates, *Phys. Rev. A*, 2006, 73(1): 013619
18. Q. T. Xie, Nonlinear floquet solutions of two periodically driven Bose–Einstein condensates, *Phys. Rev. A*, 2007, 76(4): 043622

19. X. B. Luo, Q. T. Xie, and B. Wu, Nonlinear coherent destruction of tunneling, *Phys. Rev. A*, 2007, 76(5): 051802
20. X. Luo, Q. Xie, and B. Wu, Quasienergies and floquet states of two weakly coupled Bose–Einstein condensates under periodic driving, *Phys. Rev. A*, 2008, 77(5): 053601
21. Y. H. Chen, W. Wu, G. C. Liu, H. S. Tao, and W. M. Liu, Quantum phase transition of cold atoms trapped in optical lattices, *Front. Phys.*, 2012, 7(2): 223
22. A. Eckardt, C. Weiss, and M. Holthaus, Superfluid–insulator transition in a periodically driven optical lattice, *Phys. Rev. Lett.*, 2005, 95(26): 260404
23. B. Y. Ou, X. G. Zhao, J. Liu, and S. G. Chen, Nonlinear tunneling and chaos between two Bose–Einstein condensates trapped in time-dependent potential, *Phys. Lett. A*, 2001, 291(1): 17
24. F. K. Abdullaev and R. A. Kraenkel, Coherent atomic oscillations and resonances between coupled Bose–Einstein condensates with time-dependent trapping potential, *Phys. Rev. A*, 2000, 62(2): 023613
25. C. F. Bharucha, K. W. Madison, P. R. Morrow, S. R. Wilkinson, B. Sundaram, and M. G. Raizen, Observation of atomic tunneling from an accelerating optical potential, *Phys. Rev. A*, 1997, 55(2): R857
26. A. Sibille, J. F. Palmier, and F. Laruelle, Zener interminiband resonant breakdown in superlattices, *Phys. Rev. Lett.*, 1998, 80(20): 4506
27. A. Izmalkov, M. Grajcar, E. Ilichev, N. Oukhanski, T. Wagner, H.G. Meyer, W. Krech, M. H. S. Amin, A. M. Brink, and A. M. Zagoskin, Observation of macroscopic Landau–Zener transitions in a superconducting device, *Europhys. Lett.*, 2004, 65(6): 844
28. B. D. Josephson, Possible new effects in superconductive tunnelling, *Phys. Lett.*, 1962, 1(7): 251
29. M. Albiez, R. Gati, J. Fölling, S. Hunsmann, M. Cristiani, and M. K. Oberthaler, Direct observation of tunneling and nonlinear self-trapping in a single bosonic Josephson junction, *Phys. Rev. Lett.*, 2005, 95(1): 010402
30. Y. Shin, G. B. Jo, M. Saba, T. A. Pasquini, W. Ketterle, and D. E. Pritchard, Optical weak link between two spatially separated Bose–Einstein condensates, *Phys. Rev. Lett.*, 2005, 95(17): 170402
31. A. Smerzi, S. Fantoni, S. Giovanazzi, and S. R. Shenoy, Quantum coherent atomic tunneling between two trapped Bose–Einstein condensates, *Phys. Rev. Lett.*, 1997, 79(25): 4950
32. A. Barone and G. Paterno, Physics and Applications of the Josephson Effect, New York: Wiley, 1982
33. F. P. Esposito, L. P. Guay, R. B. MacKenzie, M. B. Paranjape, and L. C. R. Wijewardhana, Field theoretic description of the Abelian and non-Abelian Josephson effect, *Phys. Rev. Lett.*, 2007, 98(24): 241602
34. R. Qi, X. L. Yu, Z. B. Li, and W. M. Liu, Non-Abelian Josephson effect between two $F = 2$ spinor Bose–Einstein condensates in double optical traps, *Phys. Rev. Lett.*, 2009, 102(18): 185301
35. M. Ueda and M. Koashi, Theory of spin-2 Bose–Einstein condensates: Spin correlations, magnetic response, and excitation spectra, *Phys. Rev. A*, 2002, 65(6): 063602
36. C. V. Ciobanu, S. K. Yip, and T. L. Ho, Phase diagrams of $F = 2$ spinor Bose–Einstein condensates, *Phys. Rev. A*, 2000, 61(3): 033607
37. R. Barnett, S. Mukerjee, and J. E. Moore, Vortex lattice transitions in cyclic spinor condensates, *Phys. Rev. Lett.*, 2008, 100(24): 240405
38. R. Barnett, A. Turner, and E. Demler, Classifying novel phases of spinor atoms, *Phys. Rev. Lett.*, 2006, 97(18): 180412
39. H. Schmaljohann, M. Erhard, and J. Kronj, Dynamics of $F = 2$ spinor Bose–Einstein condensates, *Phys. Rev. Lett.*, 2004, 92(4): 040402
40. D. M. Stamper-Kurn, M. R. Andrews, A. P. Chikkatur, S. Inouye, H. J. Miesner, J. Stenger, and W. Ketterle, Optical confinement of a Bose–Einstein condensate, *Phys. Rev. Lett.*, 1998, 80(10): 2027
41. T. Ohmi and K. Machida, Bose–Einstein condensation with internal degrees of freedom in alkali atom gases, *J. Phys. Soc. Jpn.*, 1998, 67: 1822
42. T. L. Ho, Spinor Bose condensates in optical traps, *Phys. Rev. Lett.*, 1998, 81(4): 742
43. S. Ashhab and C. Lobo, External Josephson effect in Bose–Einstein condensates with a spin degree of freedom, *Phys. Rev. A*, 2002, 66(1): 013609
44. H. T. Ng, C. K. Law, and P. T. Leung, Quantum-correlated double-well tunneling of two-component Bose–Einstein condensates, *Phys. Rev. A*, 2003, 68(1): 013604
45. A. J. Leggett, Bose–Einstein condensation in the alkali gases: Some fundamental concepts, *Rev. Mod. Phys.*, 2001, 73(2): 307
46. O. E. Mustecaplioglu, M. Zhang, and L. You, Tunneling of condensate magnetization in a double-well potential, *Phys. Rev. A*, 2005, 71(5): 053616
47. O. E. Mustecaplioglu, W. Zhang, and L. You, Quantum dynamics of a spin-1 condensate in a double-well potential, *Phys. Rev. A*, 2007, 75(2): 023605
48. M. S. Chang, C. Hamley, M. Barrett, J. Sauer, K. Fortier, W. Zhang, L. You, and M. Chapman, Observation of spinor dynamics in optically trapped ^{87}Rb Bose–Einstein condensates, *Phys. Rev. Lett.*, 2004, 92(14): 140403
49. W. M. Liu, W. B. Fan, W. M. Zheng, J. Q. Liang, and S. T. Chui, Quantum tunneling of Bose–Einstein condensates in optical lattices under gravity, *Phys. Rev. Lett.*, 2002, 88(17): 170408
50. J. Q. Liang and H. J. W. Muller-Kirsten, Bounces and the calculation of quantum tunneling effects, *Phys. Rev. D*, 1992, 45(8): 2963

51. B. P. Anderson and M. A. Kasevich, Macroscopic quantum interference from atomic tunnel arrays, *Science*, 1998, 282: 1686
52. F. S. Cataliotti, S. Burger, C. Fort, P. Maddaloni, F. Minardi, A. Trombettoni, A. Smerzi, and M. Inguscio, Josephson junction arrays with Bose–Einstein condensates, *Science*, 2001, 293(5531): 843
53. U. Weiss, Quantum Dissipative Systems, Singapore: World Scientific, 1993
54. V. V. Ivanov, A. Alberti, M. Schioppo, G. Ferrari, M. Artoni, M. L. Chiofalo, and G. M. Tino, Coherent delocalization of atomic wave packets in driven lattice potentials, *Phys. Rev. Lett.*, 2008, 100(4): 043602
55. C. F. Bharucha, K. W. Madison, P. P. Morrow, S. R. Wilkinson, B. Sundaram, and M. G. Raizen, Observation of atomic tunneling from an accelerating optical potential, *Phys. Rev. A*, 1997, 55(2): R857
56. L. S. Schulman, Techiques and Applications of Path Integration, New York: Wiley-Interscience, 1981
57. A.C. Ji, Q. Sun, X. C. Xie, and W. M. Liu, Josephson effect for photons in two weakly linked microcavities, *Phys. Rev. Lett.*, 2009, 102(2): 023602
58. P. R. Eastham, and P. B. Littlewood, Bose condensation of cavity polaritons beyond the linear regime: The thermal equilibrium of a model microcavity, *Phys. Rev. B*, 2001, 64(23): 235101
59. S. Giovanazzi, A. Smerzi, and S. Fantoni, Josephson effects in dilute Bose–Einstein condensates, *Phys. Rev. Lett.*, 2000, 84(20): 4521
60. S. Levy, E. Lahoud, I. Shomroni, and J. Steinhauer, The a.c. and d.c. Josephson effects in a Bose–Einstein condensate, *Nature*, 2007, 449(7162): 579
61. Y. Colombe, T. Steinmetz, G. Dubois, F. Linke, D. Hunger, and J. Reichel, Strong atom-field coupling for Bose–Einstein condensates in an optical cavity on a chip, *Nature*, 2007, 450(7167): 272
62. R. H. Dicke, Coherence in spontaneous radiation processes, *Phys. Rev.*, 1954, 93(1): 99
63. F. Brennecke, T. Donner, S. Ritter, T. Bourdel, M. Köhl, and T. Esslinger, Cavity QED with a Bose–Einstein condensate, *Nature*, 2007, 450(7167): 268
64. V. N. Popov and V. S. Yarunin, Collective Effects in Quantum Statistics of Radiation and Matter, Dordrecht: Kluwer Academic Publishers, 1988
65. M. J. Hartmann and G. S. L. Fernando, Strongly interacting polaritons in coupled arrays of cavities, *Nat. Phys.*, 2006, 2(12): 849
66. A. Smerzi, S. Fantoni, S. Giovanazzi, and S. R. Shenoy, Quantum coherent atomic tunneling between two trapped Bose–Einstein condensates, *Phys. Rev. Lett.*, 1997, 79(25): 4950
67. S. Raghavan, A. Smerzi, S. Fantoni, and S. R. Shenoy, Coherent oscillations between two weakly coupled Bose–Einstein condensates: Josephson effects, π-oscillations, and macroscopic quantum self-trapping, *Phys. Rev. A*, 1999, 59(1): 620
68. H. J. Kimble, Cavity Quantum Electrodynamics, edited by P. R. Berman, New York: Academic, 1994